Published in final edited form as:

Clin Nucl Med. 2014 October ; 39(10): 874–881. doi:10.1097/RLU.0000000000000539.

A pilot study of the value of 18F-Fluoro-deoxy-thymidine (18F-FLT) PET/CT in predicting viable lymphoma in residual 18F-FDG avid masses following completion of therapy

Esther Mena, MD,
Molecular Imaging Program, National Cancer Institute, Building 10, Room B3B69F, Bethesda, MD 20892

M Liza Lindenberg, MD,
Molecular Imaging Program, National Cancer Institute, Building 10, Room B3B69F, Bethesda, MD 20892

Baris I Turkbey, MD,
Molecular Imaging Program, National Cancer Institute, Building 10, Room B3B69F, Bethesda, MD 20892

Joanna Shih, PhD,
Biometric Research Branch, Division of Cancer Treatment and Diagnosis, National Cancer Institute, National Institutes of Health, Bethesda, MD, 20892

Jean Logan, PhD,
Brookhaven National Laboratories, PO Box 5000, 30 Bell Ave., Building 490, Upton, NY 11973-5000

Stephen Adler, PhD,
SAIC Contractor to NCI, Fort Detrick Frederick, MD 21702

Karen Wong,
Molecular Imaging Program, National Cancer Institute, Building 10, Room B3B69F, Bethesda, MD 20892

Wyndham Wilson, MD,
Lymphoma Therapeutics Section, Center for Cancer Research, National Cancer Institute, Building 10, Rm 4, Bethesda, MD

Peter L Choyke, MD, and
Molecular Imaging Program, National Cancer Institute, Building 10, Room B3B69F, Bethesda, MD 20892

KA Kurdziel

Corresponding Author: Karen A. Kurdziel, MD, Molecular Imaging Program, National Cancer Institute, Building 10, Room B3B69F, Bethesda, MD 20892.

Conflict of Interest Statement
The authors declare that they have no conflict of interest.

Molecular Imaging Program, National Cancer Institute, Bldg 10, Room B3B69F, Bethesda, MD 20892

Abstract

Despite its success in diagnosing and staging lymphoma, ^{18}F-FDG PET/CT can be falsely positive in areas of post-treatment inflammation. 3′-^{18}F-Fluoro-3′-deoxy-l-thymidine (^{18}F-FLT) is a structural analog of the DNA constituent thymidine; its uptake correlates with cellular proliferation. This pilot study evaluates the ability of ^{18}F-FLT PET/CT to distinguish viable lymphoma from post treatment inflammatory changes in ^{18}F-FDG-avid residual masses.

Methods—21 lymphoma patients with at least one ^{18}F-FDG avid residual mass after therapy, underwent ^{18}F-FLT PET/CT imaging. ^{18}F-FDG and ^{18}F-FLT uptake values were compared, including quantitative pharmacokinetic parameters extracted from the ^{18}F-FLT time activity curves (TACs) generated from dynamic data using graphical and non-linear compartmental modeling.

Results—The true nature of the residual mass was confirmed by biopsy in 12 patients: 8 positive and 4 negative for viable lymphoma and by followup CT and/or repeat ^{18}F-FDG PET/CT imaging over 1 year: among 9 patients 7 lesions resolved or decreased and 2 showed growth indicative of lymphoma. ^{18}F-FLT PET $SUV_{est.max}$ was significantly higher in tumors than in benign lesions (5.5±2.2 vs. 1.7±0.6; $p<0.0001$), while the difference in ^{18}F-FDG SUVs was not significant (malignant 7.8±3.8 vs. benign 5.4±2.4; $p=0.11$). All of the benign lesions had an ^{18}F-FLT $SUV_{est.max}$ less than 3.0.

Conclusion—^{18}F-FLT shows improved specificity over ^{18}F-FDG in distinguishing residual lymphoma from post treatment inflammation and may be useful in the evaluation of patients with residual ^{18}F-FDG-positive masses after completing therapy.

Keywords

PET imaging; ^{18}F-FLT; ^{18}F-FDG; Lymphoma; Residual mass; PET/CT

INTRODUCTION

Malignant lymphomas are the fifth most frequent cancer in the United States, with about 79,030 new cases expected in 2013.[1] With advances in treatments, many Hodgkin (HL) and non-Hodgkin lymphomas (NHL) are potentially curable; [2, 3] however, despite improvements in therapy, 20–50% of patients with advanced-stage HL and NHL still relapse after completion of first-line therapy [4]. Hence, accurate post-treatment characterization is crucial.

For the last few decades, computed tomography (CT) has been considered the gold standard for imaging lymphoma, providing excellent spatial resolution and the ability to measure changes in size. However, CT offers only anatomic information and thus, cannot differentiate among fibrosis, inflammation and active residual disease. Combined PET/CT using ^{18}F-fluorodeoxyglucose (^{18}F-FDG), a glucose analog, has improved upon CT alone [5] and is now an integral part of lymphoma assessment, particularly in the post-therapy setting [6]. Unfortunately, ^{18}F-FDG-PET is well known to exhibit false-positive uptake in

inflammatory or infectious processes, such as granulomatous disease, sarcoidosis, brown fat and rebound thymic hyperplasia [7] and when necrotic tumors become infiltrated by macrophages [8]. This is due to the increased glucose metabolism of macrophages and other inflammatory cellular infiltrates relative to normal tissue.

Given the high proliferative rates of most malignancies, 3′-deoxy-3′-^{18}F-Fluorothymidine (^{18}F-FLT), a structural analog of the DNA constituent thymidine, was first utilized as a proliferative marker by Shields et.al. [9]. ^{18}F-FLT is largely trapped within the cell after phosphorylation by thymidine kinase (TK1), a crucial enzyme in the proliferation pathway. Studies using tumor cell lines [10, 11] and murine xenografts [12] demonstrate that ^{18}F-FLT uptake correlates with cellular proliferation based on Ki67 staining and other measures of DNA synthesis [11]. In clinical trials, ^{18}F-FLT-PET uptake also correlates with proliferation measurements, including Ki-67, in a variety of human cancers [13–15], including lymphomas [16]. Since residual lymphoma would be expected to exhibit a high level of proliferation whereas inflammation would not, ^{18}F-FLT-PET might be suitable for distinguishing these two states.

Therefore, we investigated the ability of ^{18}F-FLT PET to distinguish between residual tumor and inflammation in ^{18}F-FDG-avid residual masses after completion of therapy for lymphoma based on the hypothesis that proliferation would be reduced in benign causes of residual mass compared to residual lymphoma.

METHODS

Patient Population and Study Design

This is a HIPAA compliant, prospective, single-institution study, approved the Institutional Review Board (IRB) and the Radiation Safety Committee. All patients gave written informed consent to participate. Inclusion criteria included subjects older than 18 years, diagnosed with T- or B-cell lymphoma, who completed therapy and demonstrated at least one residual, ^{18}F-FDG positive mass (defined as lesion uptake > mean mediastinal blood pool), which was ≥ 1.5 cm in size. Laboratory parameters were obtained within 2 weeks of ^{18}F-FLT PET/CT and included: liver enzymes, i.e. serum GOT and serum GPT < 5 fold the upper normal limit, and serum bilirubin ≤ 2 fold the upper normal limit. Exclusion criteria included severe claustrophobia, secondary malignancy, liver lesions (due to high normal FLT uptake), weight >136 kg (weight limit for scanner table), pregnancy or lactation.

Between 2009 and 2012, 21 patients (10 males, 11 females) were enrolled. Clinical post-therapy diagnostic ^{18}F-FDG PET/CT was performed at least 2-weeks (mean of 44 weeks) from completion of therapy. Patients with clinically designated positive residual mass(es) were eligible for enrollment. ^{18}F-FLT PET/CT imaging was performed within 2-weeks of clinical ^{18}F-FDG PET/CT. In 12 patients, the residual mass was biopsied after ^{18}F-FLT PET/CT imaging, and histopathology was used to define/exclude viable lymphoma. In the remaining cases, biopsy was not performed clinically and patients were followed by CT and/or ^{18}F-FDG PET/CT for a minimum of 1 year. Increases in lesion size or ^{18}F-FDG uptake >20% during that period were considered to represent residual tumor.

^{18}F-FDG PET/CT Imaging Protocol

^{18}F-FDG PET/CT images were performed following a 4-hour fast and blood glucose level < 125 mg/dl, PET/CT. Imaging was performed ~ 1 hour post injection of 10–15 mCi [375–555 MBq] of ^{18}F-FDG i.v. Eleven patients were imaged using a 3-dimensional (3D) Time-of-Flight (TOF) mode Gemini TF (Philips Medical Systems, Andover, MA, USA). The remaining 10 patients were imaged on a GE Discovery ST PET/CT, (General Electric Medical Systems, Milwaukee, WI). A low dose, non-contrast, CT transmission scan (120 kVp, 60mAs) was used for attenuation correction and co-registration purposes. To normalize for possible individual scanner quantitative SUV value differences, a tumor: mediastinal blood pool ratio was also performed. All tumors were visible over background. All tumors had ^{18}F-FDG $SUV_{est.max}$. value >2, and had a minimum tumor:mediastinal blood pool value of 1.4.

^{18}F-FLT PET/CT Imaging Protocol

All ^{18}F-FLT PET/CT imaging was performed on a 3D Philips Gemini TF camera. The images were reconstructed in the same manner described for ^{18}F-FDG PET/CT. ^{18}F-FLT synthesis was performed as described previously [17], and was obtained commercially (IBA, Sterling VA, Cardinal Health, Greenbelt, MD or PETnet pharmacies, Philadelphia, PA) using Good Manufacturing Practices (GMP) under investigational new drug (IND) No. 71,260. No specific patient preparation was required for imaging with ^{18}F-FLT. Patients received a single-bolus i.v injection of ^{18}F-FLT over 10–15 seconds, with a maximum total activity of 5 mCi [185 MBq], mean of 4.7 mCi [173.9 MBq], range 2.7–5.0 mCi [99.9–185 MBq]. The chemical ^{18}F-FLT mass dose injected was ≤ 25 nmol.

Immediately after the ^{18}F-FLT injection, dynamic PET acquisition imaging was performed for 60-minutes through the target lesion. If necessary, the patient was allowed a brief break otherwise this was then followed by a torso PET image (mid-ear to upper thigh) ~1h p.i. (range, 68–86 min. p.i.), and an additional 10 minute static image of the target lesion (single bed position) was acquired upon completion of the torso image (range, 100–127 min p.i.). Corresponding low-dose transmission CT scans (60mA, 120 KVp) were acquired before each PET emission scan. Patients were questioned regarding potential subjective adverse events during and after each ^{18}F-FLT imaging session. Venous blood samples (~5ml) were obtained at ~1h and at ~2h post injection and the simplified solid phase extraction chromatography (SepPak; Walters Corp.) developed by Shields et.al. [9] was performed to determine the fraction of parent ^{18}F-FLT present.

Imaging Analysis

The attenuation corrected PET/CT images in transaxial, coronal and sagittal projection planes were evaluated visually and co-registered with the CT and displayed using MIM 5.2 (Cleveland, OH, USA) by two experienced nuclear medicine physicians, blinded to the histopathology results and clinical follow-up.

Complete dynamic data sets were available in 13 patients and all patients had static imaging. In each patient a single target tumor lesion was selected for quantitative analysis. In an effort to reduce dominance by statistical noise, an estimated maximum Standardized Uptake Value

($SUV_{est.max}$) was defined as the mean SUV value of the 20% "hottest" pixels, using an automated 80% maximum pixel value within a VOI containing the entire lesion. Manually drawn VOIs were drawn within in the largest vascular structure in the field of view (~0.4 cm diameter), in the liver (~3 cm), in the muscle (~2.5 cm) and in the bone marrow (~1.0 cm); SUV_{mean} of each was used to create reference normal tissue TACs and blood input functions.

Dynamic Analysis

For kinetic analysis, ^{18}F-FLT TACs were generated for all evaluable 60-minute dynamic patient data sets (n=13) based on VOIs drawn on the summed images. Image derived input functions were created from the vascular VOI TACs. To reduce noise, these image-derived input functions were fitted to 1 or 2 exponentials as appropriate. (Figure 5) The lesion data was fit to a 2-compartment irreversible model. K_1 refers to the rate of transfer from venous blood to lesion and k_2 is the inverse transfer. For an irreversible tracer, the parameter k_3 is a function of the available binding, in this case presumably to TK1.[10] In addition $\lambda k3$ was calculated, where $\lambda=K_1/k_2$, which compensates for the intrinsic correlation between k_2 and k_3[18].

The dynamic images were also analyzed using the Patlak graphical method (Figure 5), again assuming irreversible binding, using the K_i parameter. [19] λ k_3, K_i, $SUV_{est.max}$., and various combinations of SUV to reference regions and time points (i.e. 30 min, ~1hr, and ~2hr parameters) were used in receiver operator characteristic (ROC) analyses to determine the best parameter to differentiate between a malignant and benign lesion based on ^{18}FLT PET/CT imaging.

Statistical Analysis

Statistical analyses were performed using R and SPSS software. Quantitative values were expressed as mean ± SD, and range. The two sample Wilcoxon signed-rank test with a significance level of $p < 0.05$ was used to compare the differences in ^{18}F-FDG and ^{18}F-FLT uptake between benign and tumor masses. Pathology and/or clinical imaging follow-up were used to establish the final diagnosis of each lesion. The receiver operating characteristic (ROC) analysis of ^{18}F-FDG and ^{18}F-FLT SUV uptake was performed using the final diagnosis as the gold standard. The area under the curve (AUC) and its standard error were estimated for each ROC analysis. For the purpose of differentiating between benign and malignant tumors, $SUV_{est.max}$ value, which maximized the sum of sensitivity and specificity, was used as the $SUV_{est.max}$ cut-off value. Association between tumor size and SUV uptake was tested based on the Wald's test from the fitted linear model.

RESULTS

Clinical findings

The study population consisted of 21 previously treated lymphoma patients (mean age, 46 yrs; range 19 to 75yrs), with HL (n=5) and NHL (n=16), Stage II to IV, all of whom had residual disease after treatment suspected by ^{18}F-FDG PET/CT. Target lesions were localized either supradiaphragmatic (n=9) or subdiaphragmatic (n=12). The mean target

lesion size was 3.4 ± 2.1 cm. (range 1.6 to 9cm). Patient characteristics and results are summarized in Table 1.

All ^{18}F-FLT injections were well tolerated with no adverse events. The average inter-scan interval between the ^{18}F-FDG and ^{18}F-FLT PET/CT scans was 4.4 ± 0.7 days; (range 1 to 13 days.)

Of the 21 evaluable target tumor lesions, 11 were identified as non-malignant by pathology (inflammation (n=1), granuloma (n=1), infection (n=1) and sarcoidosis (n=1)), or by clinical/imaging follow-up (n=7). Ten were determined to be recurrent lymphomatous masses based on histopathology (n=7) or clinical/imaging follow-up (n=3).

^{18}F-FDG Findings

As defined for entry into this study, all patients had an ^{18}F-FDG-positive residual mass, defined as visibly increased ^{18}F-FDG uptake within a lesion which had a $SUV_{est.max}$ greater than that of mediastinal blood pool. This ratio was used to reduce any potential quantitative effects resulting from different PET scanners. Only 11 of the 21 ^{18}F-FDG-positive PET/CT residual masses proved to be true-positives for recurrent tumor. The remaining 10 ^{18}F-FDG avid lesions were false-positive and represented a range of benign lesions. The difference in ^{18}F-FDG-$SUV_{est.max}$ between benign processes (5.4±2.4, range 2.1–10.4) and residual lymphomatous lesions (7.3±3.8, range 3.8–15.8) was not statistically significant, p=0.11. Figure 1.

^{18}F-FLT Imaging

Mean TACs for both benign and malignant lesions, Figure 2, showed a rapid uptake of ^{18}F-FLT within lymphomas, with ~90% of the activity reaching a peak at 5 to 10 min. post-injection. Tumor uptake remained higher than that of blood pool, with some tumors exhibiting a continued slow uptake throughout the remaining 50 minutes of the dynamic scan, and others showing a relative plateau after 10 minutes. There was a significant difference in the mean λk_3 values between the benign (0.0251±0.009) and malignant lesions (0.0603±0.026), p=0.01, using the standard t-test. The higher λk_3 values in the malignant lesions are consistent with the expectation of higher TK1 binding.

Metabolite analysis revealed the two expected FLT radioactive components, ^{18}F-FLT and ^{18}F-FLT-glucuronide. The average fraction of labeled metabolites was 23.2±5.9% at ~1h p.i., and 27.3±8.0% at ~2h p.i. The average fraction of radioactivity in the plasma attributed to unchanged ^{18}F-FLT, at ~1 hour after injection, was 76.8%±7.8%; range, 64.9%–87.5%. This resulted in a minor metabolite correction in the kinetic parameters estimates. The average decay curve of the metabolites were fitted with an exponential using the MatLab software code “root” (root.cern.ch) and the $t_{1/2}$ of the fit was used for the metabolite correction (Figure 5A).

Patlak graphical analysis using both metabolite-corrected (Figure 5B) and uncorrected blood input functions was used to estimate K_i and evaluate its discriminating power between benign and malignant lesions. The metabolite corrected average K_i value was 0.045+/− 0.024 for malignant lesions and 0.017+/−0.022 (p=0.01) for benign lesions. The non-

metabolite corrected K_i estimate was 0.038 +/− 0.023 for malignant lesions and 0.013 +/ − 0.021 (p=0.02) for benign lesions. The measured area under the ROC curve for the metabolite corrected K_i was 0.86 vs. 0.83 for the non-metabolite corrected estimate. This 3% difference suggests that metabolite analysis, with its attendant requirement for repeated blood sampling, probably is unnecessary.

In order to develop practical imaging evaluation methods, single time point SUV analysis also showed the ability of ^{18}F-FLT to distinguish benign and malignant lesions by 30 min (p=0.0083), ~1h (p=0.0003) and ~2h p.i. (p=0.0028) Figure 1. Mean TACs for the benign and malignant lesions (n=13) are shown in Figure 2, showing clear separation of the curves despite a similar overall shape, with the final mean time point showing a slight decrease, possibly representing a small amount of late reversibility. SUVs derived from the 80 minute p.i. scan showed the greatest degree of uptake and distinction between benign and malignant lesions, but for clinical purposes, the 60 minute timepoint is just as distinct.

The average ^{18}F-FLT PET $SUV_{est.max}$. of residual tumors was significantly higher than benign lesions (5.5±2.2 vs. 1.7±0.6; p<0.0001). Figure 3 shows illustrative cases for ^{18}F-FLT uptake in malignant, (**A**) benign, (**B**) and the single ^{18}F-FLT false-negative finding (**C**); a large 9.0 × 4.9 cm. left pelvis mass, which was positive for tumor by biopsy, showing residual ALK negative anaplastic large cell lymphoma, a rare type of NHL that did not show increased ^{18}F-FLT uptake (SUV=1.6). There were nine true positive ^{18}F-FLT target lesions, either with histopathology confirmation (n=6) or clinical/imaging follow-up (n=3), and all demonstrated ^{18}F-FLT SUV values >3.0. Benign masses (n=11) typically showed no or very mild visual FLT uptake (average ^{18}F-FLT-$SUV_{est.max}$ 1.7±0.6 (range, 0.5–2.5). There was no association between tumor size and ^{18}F-FLT-$SUV_{est.max}$ using the Wald's test from the fitted linear model (p>0.05).

In addition to high uptake in residual tumors, physiologic ^{18}F-FLT uptake was also observed within the bone marrow (average SUV_{mean}, 7.3±3.3; range 2.5–14.6) as well as within the liver, (average SUV_{mean} of 4.3±1.2; range, 2.5–6.5). The average ^{18}F-FLT SUV_{mean} for muscle was 0.6±0.1 (range, 0.3–0.8).

On average, ^{18}F-FDG SUVs were greater than ^{18}F-FLT SUVs in lymphomas (7.8±3.8 vs. 5.5±2.2), with the exception of one patient that showed a slightly higher ^{18}F-FLT SUV; however the ^{18}F-FDG uptake was often high in non-malignant tissues resulting in 11 false positive lesions.

Using ROC analysis, ^{18}F-FLT $SUV_{est.max}$ distinguished between lymphoma and inflammation with a larger AUC than ^{18}F-FDG-$SUV_{est.max}$ (0.94±0.057 vs. 0.69±0.12), at ~ 1h p.i. Figure 4. This result is similar to those obtained using more complicated kinetic approaches. Appling a cut-off $SUV_{est.max}$ of 3.0 for ^{18}F-FLT to predict malignancy after treatment provided a sensitivity of 90% and specificity of 100%. The raw ^{18}F-FLT tumor uptake showed rapid separation from that of blood pool, Figure 5A, and the linearity of a Patlak Graphical Analysis, Figure 5B, indicates irreversible binding early on.

DISCUSSION

Evaluation of therapy response is crucial in the management of patients with high-grade lymphoma as patients with refractory disease are switched to salvage regimens of chemotherapy or autologous stem cell transplantation with curative intent. [20] Outside of clinical trials, CT, MRI and ultrasound are primarily used in staging, usually 6 to 8-weeks after the initiation of therapy. Difficulties in distinguishing residual tumor from fibro-necrotic tissue after therapy have been partly overcome by ^{18}F-FDG PET as fibrosis uses only minimal amounts of glucose. According to results from a meta-analysis by Zijlstra et al. [21], the sensitivity and specificity of ^{18}F-FDG-PET for detection of residual disease after completion of first-line therapy were 84% and 90%, respectively, for HL, and 72% and 100%, respectively, for aggressive NHL. However, the high rate of ^{18}F-FDG false positive results (30–50%) raises significant clinical concerns [22, 23] as the patient may receive unwarranted additional therapy when the ^{18}F-FDG PET is falsely positive [24]. With the goal of reducing these false positive findings without resorting to invasive biopsy procedures, several PET radiotracers are being developed. Recently, the thymidine analogue ^{18}F-FLT has been suggested as an in-vivo marker of a tumor's proliferative activity and possibly as a more specific tumor-imaging agent. Several groups have addressed the feasibility of studying ^{18}F-FLT PET in numerous types of cancers [13, 25–27] including lymphoma [16]. ^{18}F-FLT uptake by lymphoma cells has been shown to closely reflect the S phase of the cell cycle [10]. Wagner et al. [12] found a close correlation between ^{18}F-FLT values and the Ki-67 labeling index in implanted xenografts based on human tumor cell lines ($r=0.95$, $p<0.005$) and in patients with indolent and aggressive lymphoma, suggesting that ^{18}FLT PET imaging could assess the proliferation rate in lymphoma. Similarly, Buck et al. [16] reported a significant correlation of ^{18}F-FLT uptake and proliferation fraction by Ki-67 immunohistochemistry in biopsied tissues ($r = 0.84$; $p < 0.0001$) in 34 lymphoma patients. Most of the ^{18}F-FLT studies in lymphoma have suggested the use of ^{18}F-FLT for monitoring tumor proliferation and earlier detection of tumor response [28, 29], but limited data exists regarding the evaluation of residual masses after completion of therapy [30]. While Kasper et.al. [30] were able to show that ^{18}F-FLT uptake alone was able to predict overall survival, they did not show an advantage to combined ^{18}F-FDG/^{18}F-FLT imaging. Our study addresses a different question as we included only patients with ^{18}F-FDG positive residual masses after completion of therapy. We recognize that ^{18}F-FDG is likely to remain the primary PET-based imaging modality for lymphoma in the near future. However, our data demonstrates the utility of ^{18}F-FLT in selected cases to differentiate between residual lymphoma and benign disease in patients with residual ^{18}F-FDG positive masses. Thus, ^{18}F-FLT is considered an adjunct to, rather than a replacement for, ^{18}F-FDG.

In our cohort all but one of the true malignant lesions were detected by ^{18}F-FLT, which gives ^{18}F-FLT PET a slightly lower sensitivity than ^{18}F-FDG PET. This is concordant with previous publications, where ^{18}F-FDG was found to detect more lesions than ^{18}F-FLT [30] but at a lower specificity. In this study, the one ^{18}F-FLT false negative ($SUV_{est.max.}$ 1.7) was an ALK negative anaplastic large T-cell lymphoma which is known to have a tendency to proliferate, inhibit apoptosis and alter cytotoxic receptor signaling so the relatively low ^{18}F-

FLT uptake may be due to “proliferative stunning” as the ^{18}F-FLT scan was performed just 15 days after completion of chemotherapy and 1 day after ^{18}F-FDG PET/CT. [31]

By contrast, Buck et al [16] found that ^{18}F-FLT detected more lymphoma than the routine clinical staging imaging (490 vs. 420) in histologically proven malignant lymphoma patients. In this setting, it has been reported that ^{18}F-FLT uptake is significantly higher in aggressive lymphoma compared with indolent lymphoma (average SUV of 5.9 vs. 2.3) ($P<0.001$). Preclinical data suggests that TK1 activity is three to four times higher in malignant cells than in benign cells [32]. Similarly, Van Waarde et al. [33] studied a rat model with tumor and inflammation, confirming that inflammation was not visible with ^{18}F-FLT, and that the selectivity of ^{18}F-FLT for tumor was higher than that of ^{18}F-FDG (10.6 vs. 3.5, at 120 min post-injection). While our study did not result in any ^{18}F-FLT false-positive findings, ^{18}F-FLT false-positive findings have been reported in non-metastatic reactive lymph nodes in squamous cell carcinoma of the head and neck [25]. Increased active proliferation of B-lymphocytes in germinal centers may account for such false-positive ^{18}F-FLT uptake.

Various SUV thresholds for ^{18}F-FLT have been evaluated as a means of differentiating malignancy from benign processes, or between grades of malignancy. For example, Buck et al. presented a cut-off value of 3 to differentiate between aggressive and indolent lymphoma [16]. Similarly, in our cohort of treated patients, a cut-off $SUV_{est.max}$ of 3.0 was able to discriminate between benign and malignant processes with a sensitivity and specificity of 90% and 100%, respectively. Other series have defined a diagnosis of lymphoma disease based on a minimum threshold SUV of 1.5 [30]. This much lower threshold value was most likely chosen to achieve a better sensitivity for ^{18}F-FLT, although it also would decrease the specificity of the agent.

The kinetics of ^{18}F-FLT in tumor tissue is best described by a two-compartment model (Figure 5) [15, 29, 30]. Our result is in accordance with previous reports [33, 34] showing rapid tracer accumulation in the first 5–10 min followed by stable tracer retention. However, our study also showed that the $SUV_{est.max}$ at <1h p.i was sufficient to distinguish between tumor and benign lesions. Although the λk_3 parameter derived from a non-linear fit of dynamic data and the AUC of the ROC derived from the dynamic data had comparable results, the $SUV_{est.max}$ achieved the same results without scanning dynamically or scanning at 2 hours, p.i., thus greatly simplifying the procedure. Moreover, based on the Patlak graphical model K_i (Figure 5) to test the impact of metabolite corrections, it is clear there is little benefit to metabolite correction.

There are several limitations to this study. The relatively small number of patients (n=21) with wide heterogeneity in both Hodgkin and non-Hodgkin lymphomas did not allow for analysis based on histologic subtype. Furthermore, correlation with immunohistochemical index of cell proliferation was not performed. The small number of patient’s is also likely a contributing factor for the lack of no false positive findings. Despite these limitations there is still significant statistical power to evaluate the ability of ^{18}F-FLT PET/CT to detect residual malignancy in patients with residual ^{18}F-FDG positive residual masses following therapy.

Larger multi-center studies focusing on the various lymphoma types are still needed for confirmation.

CONCLUSION

In patients with ^{18}F-FDG-positive residual masses after therapy for lymphoma, ^{18}F-FLT PET/CT, was able to correctly identify all 10/21 subjects who did not have residual malignancy. In this small pilot study, a single time point, ^{18}F-FLT PET/CT SUV at ~1-hour post injection, had 90% sensitivity and 100% specificity for residual disease. This data suggests that larger studies of the utility of ^{18}F-FLT PET/CT in evaluating lymphoma patients with residual ^{18}FDG avid masses after completion of therapy may be beneficial.

References

1. Siegel R, Naishadham D, Jemal A. Cancer statistics, 2013. CA: a cancer journal for clinicians. 2013; 63:11–30. [PubMed: 23335087]
2. Connors JM. State-of-the-art therapeutics: Hodgkin's lymphoma. Journal of clinical oncology: official journal of the American Society of Clinical Oncology. 2005; 23:6400–6408. [PubMed: 16155026]
3. Coiffier B. State-of-the-art therapeutics: diffuse large B-cell lymphoma. Journal of clinical oncology: official journal of the American Society of Clinical Oncology. 2005; 23:6387–6393. [PubMed: 16155024]
4. Quddus F, Armitage JO. Salvage therapy for Hodgkin's lymphoma. Cancer journal (Sudbury, Mass). 2009; 15:161–163.
5. Naumann R, Vaic A, Beuthien-Baumann B, et al. Prognostic value of positron emission tomography in the evaluation of post-treatment residual mass in patients with Hodgkin's disease and non-Hodgkin's lymphoma. Br J Haematol. 2001; 115:793–800. [PubMed: 11843811]
6. Juweid ME, Stroobants S, Hoekstra OS, et al. Use of positron emission tomography for response assessment of lymphoma: consensus of the Imaging Subcommittee of International Harmonization Project in Lymphoma. J Clin Oncol. 2007; 25:571–578. [PubMed: 17242397]
7. Metser U, Even-Sapir E. Increased (18)F-fluorodeoxyglucose uptake in benign, nonphysiologic lesions found on whole-body positron emission tomography/computed tomography (PET/CT): accumulated data from four years of experience with PET/CT. Semin Nucl Med. 2007; 37:206–222. [PubMed: 17418153]
8. Kubota R, Yamada S, Kubota K, et al. Intratumoral distribution of fluorine-18-fluorodeoxyglucose in vivo: high accumulation in macrophages and granulation tissues studied by microautoradiography. J Nucl Med. 1992; 33:1972–1980. [PubMed: 1432158]
9. Shields AF, Grierson JR, Kozawa SM, et al. Development of labeled thymidine analogs for imaging tumor proliferation. Nucl Med Biol. 1996; 23:17–22. [PubMed: 9004909]
10. Rasey JS, Grierson JR, Wiens LW, et al. Validation of FLT uptake as a measure of thymidine kinase-1 activity in A549 carcinoma cells. J Nucl Med. 2002; 43:1210–1217. [PubMed: 12215561]
11. Schwartz JL, Tamura Y, Jordan R, et al. Monitoring tumor cell proliferation by targeting DNA synthetic processes with thymidine and thymidine analogs. J Nucl Med. 2003; 44:2027–2032. [PubMed: 14660729]
12. Wagner M, Seitz U, Buck A, et al. 3′-[18F]fluoro-3′-deoxythymidine ([18F]-FLT) as positron emission tomography tracer for imaging proliferation in a murine B-Cell lymphoma model and in the human disease. Cancer Res. 2003; 63:2681–2687. [PubMed: 12750297]
13. Vesselle H, Grierson J, Muzi M, et al. In vivo validation of 3′deoxy-3′-[(18)F]fluorothymidine ([(18)F]FLT) as a proliferation imaging tracer in humans: correlation of [(18)F]FLT uptake by positron emission tomography with Ki-67 immunohistochemistry and flow cytometry in human lung tumors. Clin Cancer Res. 2002; 8:3315–3323. [PubMed: 12429617]

14. Bading JR. Kinetic analysis of 18F-FLT PET in lung tumors. J Nucl Med. 2012; 53:506. author reply 506–507. [PubMed: 22294484]
15. Eckel F, Herrmann K, Schmidt S, et al. Imaging of proliferation in hepatocellular carcinoma with the in vivo marker 18F-fluorothymidine. J Nucl Med. 2009; 50:1441–1447. [PubMed: 19690030]
16. Buck AK, Bommer M, Stilgenbauer S, et al. Molecular imaging of proliferation in malignant lymphoma. Cancer Res. 2006; 66:11055–11061. [PubMed: 17108145]
17. Machulla HJ, B A, Kuntzsch M, Piert M, Wei R, Grierson JR. Simplified labeling approach for synthesizing 3′-deoxy-3′-[18F]fluorothymidine ([18F]FLT). J Radioanal Nucl Chem. 2000; 24:843–846.
18. Fowler JS, Logan J, Azzaro AJ, et al. Reversible inhibitors of monoamine oxidase-A (RIMAs): robust, reversible inhibition of human brain MAO-A by CX157. Neuropsychopharmacology. 2010; 35:623–631. [PubMed: 19890267]
19. Patlak CS, Blasberg RG. Graphical evaluation of blood-to-brain transfer constants from multiple-time uptake data. Generalizations. J Cereb Blood Flow Metab. 1985; 5:584–590. [PubMed: 4055928]
20. Kuruvilla J, Keating A, Crump M. How I treat relapsed and refractory Hodgkin lymphoma. Blood. 2011; 117:4208–4217. [PubMed: 21263152]
21. Zijlstra JM, Lindauer-van der Werf G, Hoekstra OS, et al. 18F-fluoro-deoxyglucose positron emission tomography for post-treatment evaluation of malignant lymphoma: a systematic review. Haematologica. 2006; 91:522–529. [PubMed: 16585017]
22. Terasawa T, Lau J, Bardet S, et al. Fluorine-18-fluorodeoxyglucose positron emission tomography for interim response assessment of advanced-stage Hodgkin's lymphoma and diffuse large B-cell lymphoma: a systematic review. J Clin Oncol. 2009; 27:1906–1914. [PubMed: 19273713]
23. Kostakoglu L, Schoder H, Johnson JL, et al. Interim [(18)F]fluorodeoxyglucose positron emission tomography imaging in stage I-II non-bulky Hodgkin lymphoma: would using combined positron emission tomography and computed tomography criteria better predict response than each test alone? Leuk Lymphoma. 2012; 53:2143–2150. [PubMed: 22421007]
24. El-Galaly TC, Mylam KJ, Brown P, et al. Positron emission tomography/computed tomography surveillance in patients with Hodgkin lymphoma in first remission has a low positive predictive value and high costs. Haematologica. 2012; 97:931–936. [PubMed: 22207683]
25. Troost EG, Bussink J, Oyen WJ, et al. 18F-FDG and 18F-FLT do not discriminate between reactive and metastatic lymph nodes in oral cancer. J Nucl Med. 2009; 50:490–491. [PubMed: 19223420]
26. Chen W, Cloughesy T, Kamdar N, et al. Imaging proliferation in brain tumors with 18F-FLT PET: comparison with 18F-FDG. J Nucl Med. 2005; 46:945–952. [PubMed: 15937304]
27. Visvikis D, Francis D, Mulligan R, et al. Comparison of methodologies for the in vivo assessment of 18FLT utilisation in colorectal cancer. Eur J Nucl Med Mol Imaging. 2004; 31:169–178. [PubMed: 15129698]
28. Herrmann K, Buck AK, Schuster T, et al. Predictive value of initial 18F-FLT uptake in patients with aggressive non-Hodgkin lymphoma receiving R-CHOP treatment. J Nucl Med. 2011; 52:690–696. [PubMed: 21498532]
29. Graf N, Herrmann K, Numberger B, et al. [18F]FLT is superior to [18F]FDG for predicting early response to antiproliferative treatment in high-grade lymphoma in a dose-dependent manner. Eur J Nucl Med Mol Imaging. 2013; 40:34–43. [PubMed: 23053327]
30. Kasper B, Egerer G, Gronkowski M, et al. Functional diagnosis of residual lymphomas after radiochemotherapy with positron emission tomography comparing FDG- and FLT-PET. Leuk Lymphoma. 2007; 48:746–753. [PubMed: 17454633]
31. Kinney MC, H R, Medina EA. Anaplastic Large Cell Lymphoma: Twenty-five years of discovery. Arch Pathol Lab Med. 2011; 135:19–43. [PubMed: 21204709]
32. Boothman DA, Davis TW, Sahijdak WM. Enhanced expression of thymidine kinase in human cells following ionizing radiation. Int J Radiat Oncol Biol Phys. 1994; 30:391–398. [PubMed: 7928466]
33. van Waarde A, Cobben DC, Suurmeijer AJ, et al. Selectivity of 18F-FLT and 18F-FDG for differentiating tumor from inflammation in a rodent model. J Nucl Med. 2004; 45:695–700. [PubMed: 15073267]

34. Pio BS, Park CK, Pietras R, et al. Usefulness of 3′-[F-18]fluoro-3′-deoxythymidine with positron emission tomography in predicting breast cancer response to therapy. Mol Imaging Biol. 2006; 8:36–42. [PubMed: 16362149]

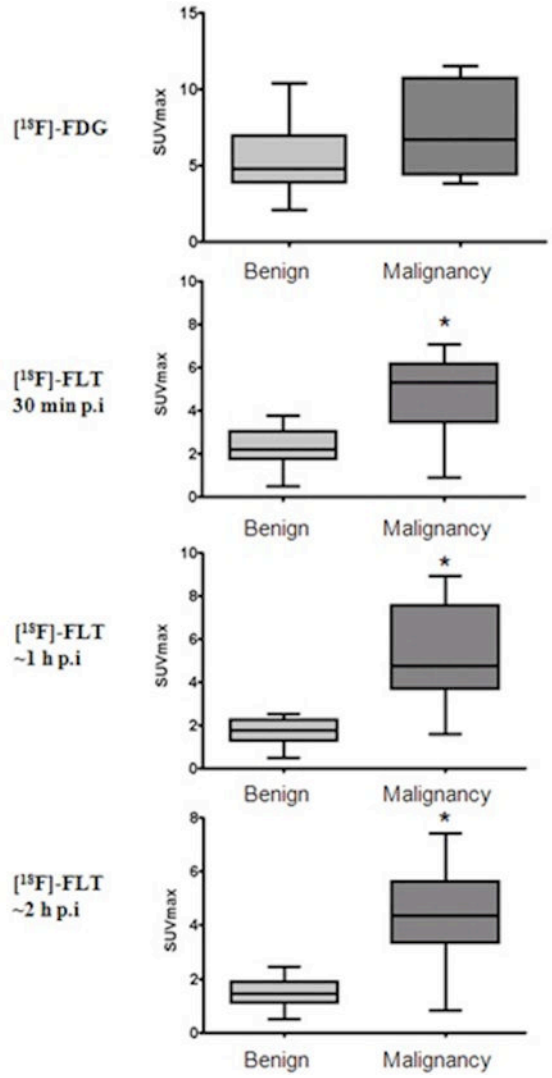

Figure 1.

Bar graphs of the average $SUV_{est.max}$ values for ^{18}F-FDG at 1h p.i. and for ^{18}F-FLT at 3 different time points (30 min, ~1h and ~2 h p.i.). The brackets are the $SUV_{est.max.}$ range at each time point, the grey boxes are the standard deviation (lighter grey the benign, darker grey malignant) and the line within the box is the average $SUV_{est.max}$. Overlap of ^{18}F-FDG-$SUV_{est.max}$ uptake was observed in non-malignant processes (5.4±2.4) and residual lymphoma (7.8±3.8), (p=0.11). Discrimination between non-malignant and residual lymphoma lesions was seen with ^{18}F-FLT with statistical significance (*) at all time points; at 30 min (p=0.0078), at ~ 1 hour (p<0.0001) and at ~2 hours p.i. (p=0.0038).

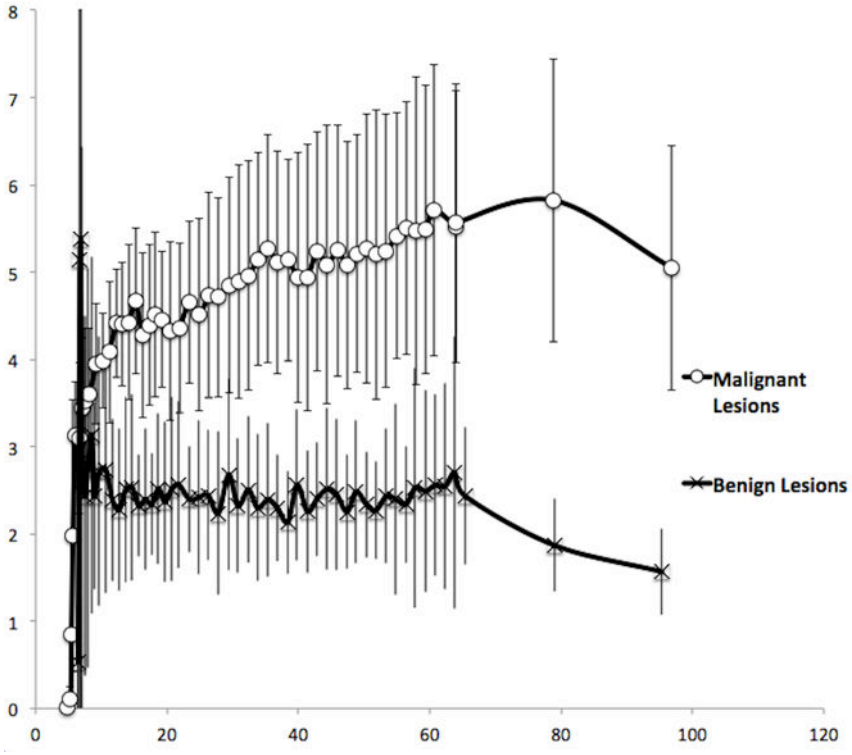

Figure 2.

Mean benign and mean malignant lesion ^{18}F-FLT Time–activity-curves. Solid vertical lines represent standard deviation value. While the greatest magnitude of difference appears at ~80min, when the ^{18}F-FLT appears to begin to wash out of the benign lesions, good differentiation is also notable at earlier time points as well.

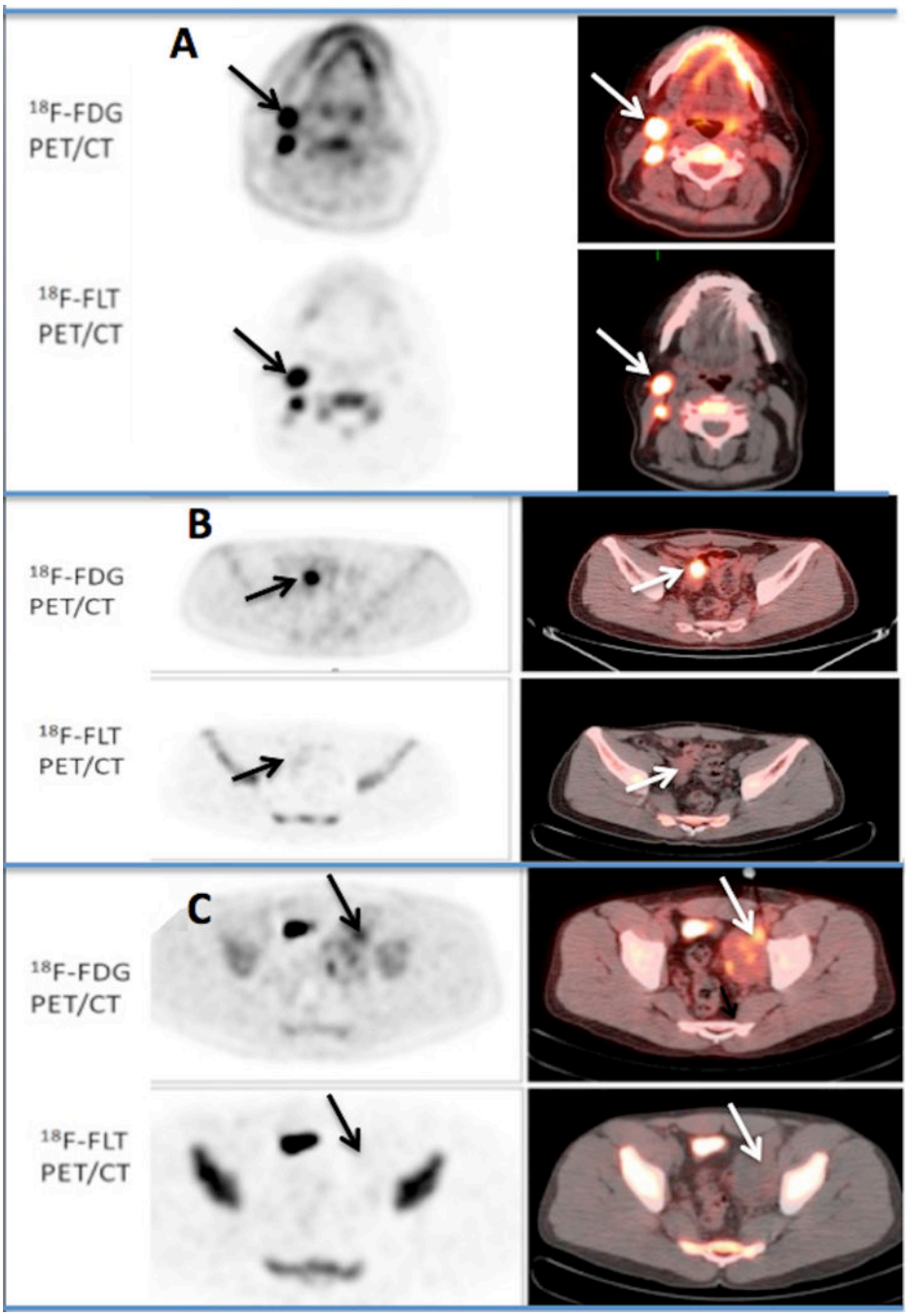

Figure 3. shows illustrative cases for ^{18}F-FLT uptake in malignant (A), benign (B), and the single ^{18}F-FLT false-negative finding (C), a large 9.0 × 4.9 cm left pelvis mass

A: Transaxial PET and fused PET/CT images, equivalently scaled with a color cut-off intensity of 2.5 in a 49 year-old man with a history of non-Hodgkin B-cell lymphoma with residual enlarged right cervical lymph nodes after 6 cycles of chemotherapy. Both ^{18}F-FDG and^{18}F-FLT PET/CT scans at ~1h p.i. show persistent high uptake ($SUV_{est.max}$ of 8.7 and of 11.4 respectively Post-treatment biopsy confirmed the presence of residual B-cell lymphoma.

B: Transaxial pelvis ^{18}F-FDG and ^{18}F-FLT PET/CT images in a 38 year-old male, performed within 3 days of each other and 5.3 weeks following the completion of EPOCH-R therapy for non-Hodgkin B-cell lymphoma (equivalently scaled with an SUV color cut off on the fused images of 2.5) demonstrating a residual 2.2 cm. mass with an FDG $SUV_{est.max}$ 10.3 within the small bowel, extending to the posterior bladder. ^{18}F-FLT PET/CT was visually interpreted as negative, with only mild uptake ($SUV_{est.max}$ 2.3). Histopathology demonstrated the presence of fibrosis and chronic inflammatory changes associated with an enterovesicular fistula.

C: 27-year-old man with history of non-Hodgkin (NHL) lymphoma with residual large left pelvic mass after completion of EPOCH chemotherapy. The images are equivalently scaled with an SUV color cut-off of 2.5 on the fused PET/CT images (right). ^{18}F-FDG PET/CT shows heterogeneous residual uptake ($SUV_{est.max}$ 3.8). ^{18}F-FLT visually showed no corresponding uptake ($SUV_{est.max}$ 1.6). Biopsy confirmed the presence of residual ALT negative anaplastic large cell lymphoma, a rare type of NHL. This was the only false negative ^{18}F-FLT in our series and could possibly be due to proliferative stunning as the ^{18}F-FLT imaging was performed 15 days after completion of 6-cycles of EPOCH chemotherapy (the ^{18}F-FDG PET/CT was performed 1-day prior to the ^{18}F-FLT PET/CT. Intense activity in the right mid-anterior pelvis is a portion of the bladder.

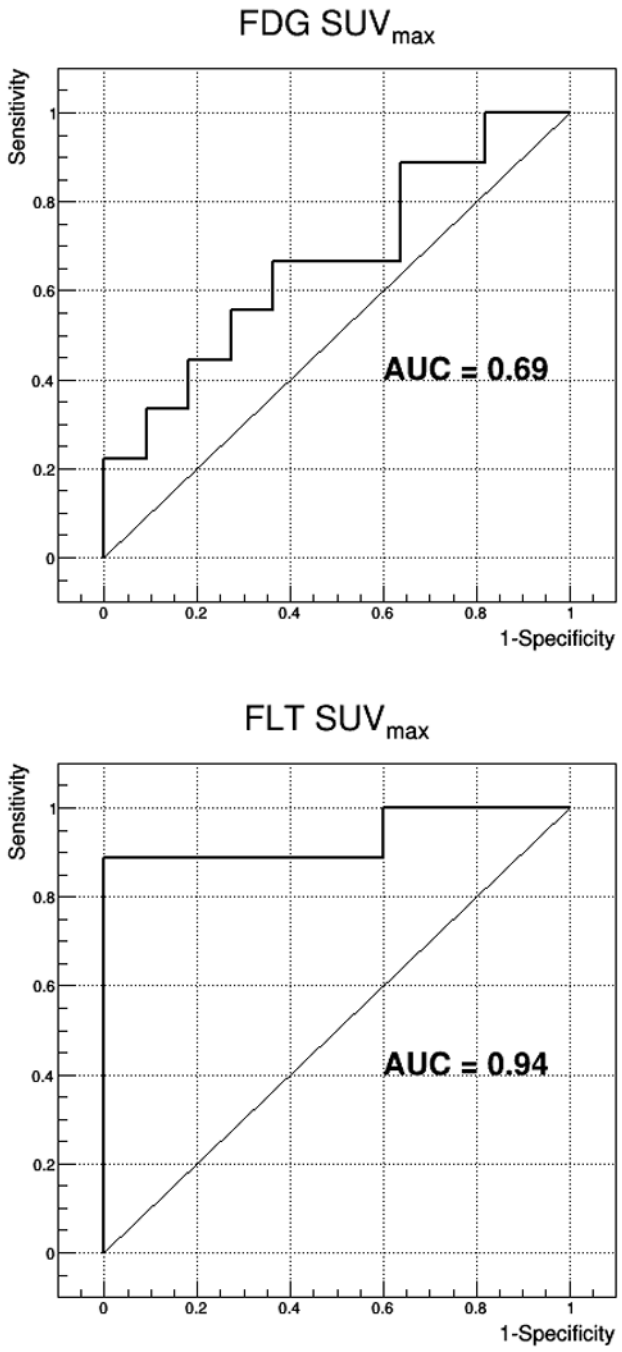

Figure 4.

Using receiver operating characteristic (ROC) analysis, ^{18}F-FLT-SUV$_{est.max}$ distinguished between lymphoma and benign lesions with a larger area under the AUC) and that of ^{18}F-FDG-SUV$_{est.\ max}$ (0.94 vs. 0.69), at ~1h p.i. curve

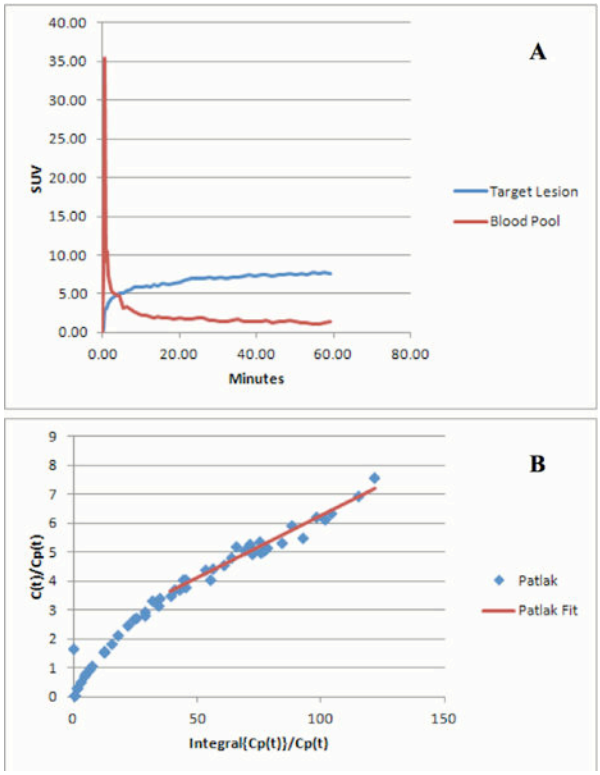

Figure 5.

Figure A shows the ^{18}FLT Time–activity-curve representing the average of all tumor target lesions, in which uptake is expressed in $SUV_{est.max}$. Lymphoma showed rapid uptake of ^{18}FLT, peaking at approximately 5 to 10, followed by relative plateau. **Figure B** shows the Patlak graphical analysis plot. Note the linearity consistent with irreversible binding.

Table 1

Patients' characteristics (n=21)

Patient	Age/Sex	Diagnosis	Residual Mass/Size (cm)	^{18}FDG ^{1}SUV$_{est.max}$/^{2}Tumor: Blood Pool	^{18}FLT SUV$_{est.\ max}$	Diagnosis/Method
1	40/F	NHL (mediastinal gray zone lymphoma; Sarcoid)	Right hilum LN (2.4 cm)	4.6/4.1	0.7	Benign/FU
2	50/F	NHL (DLBCL; HIV +)	Superior mediastinal LN (2.4 cm)	8.4/4.6	2.0	Benign/FU
3	34/F	HL	Lumbar Vertebrae (2.5 cm)	10.1/7.5	8.9	Malignant/FU
4	27/M	NHL (Anaplastic large cell lymphoma)	Right pelvic mass (9.0 cm)	3.8/3.6	1.6	Malignant/Bx
5	19/F	NHL (Peripheral T-cell lymphoma)	Intercostal soft tissue mass (2.3 cm)	6.9/4.4	1.3	Benign/Bx
6	49/M	NHL (Plasma cell neoplasm: Gamma heavy chain disease)	Right cervical LN (3.7 cm)	6.7/5.5	7.5	Malignant/Bx
7	31/F	HL	Anterior mediastinal mass (2.7 cm)	5.4/5.8	3.4	Malignant/Bx
8	42/M	NHL (DLBCL)	Anterior mediastinal mass (6.8 cm)	4.7/4.0	1.6	Benign/FU
9	28/M	HL	Internal right iliac LN (2.2 cm)	4.6/3.0	6.5	Malignant/FU
10	38/M	NHL (DLBCL)	Right pelvic mass (2.2 cm)	10.3/6.1	2.3	Benign/Bx
11	48/M	NHL (DLBCL)	Right paratracheal LN (2.0 cm)	4.8/2.9	2.5	Benign/Bx
12	40/M	NHL (Anaplastic large cell lymphoma)	Left inguinal LN (1.6 cm)	3.8/1.9	2.2	Benign/Bx
13	58/F	NHL (chronic lymphocytic leukemia)	Left axilla LN (3.0 cm)	4.0/2.9	7.6	Malignant/Bx
14	51/F	NHL (DLBCL)	Gastrohepatic LN (2.8 cm)	6.9/4.8	4.5	Malignant/Bx
15	52/F	NHL (Adult T-cell Leukemia; HTLV-1)	Right posterior thigh mass (2.5 cm)	6.4/4.0	1.9	Benign/FU
16	67/F	NHL (DLBCL)	Left abdominal mass (8.0 cm)	15.8/11.5	3.9	Malignant/Bx
17	39/M	NHL (DLBCL; HIV +)	Left suprarenal mass (4.3 cm)	11.2/8.1	4.7	Malignant/FU
18	69/F	NHL (DLBCL)	Splenic mass (2.3 cm)	2.1/1.4	0.5	Benign/FU
19	49/F	HL	Right paraaortic LN (2.7 cm)	3.8/1.8	1.1	Benign/FU
20	75/M	HL	Right hilum LN (1.6 cm)	3.5/1.5	1.5	Benign/FU
21	62/M	NHL (DLBCL)	Mesenteric mass (5.2 cm)	9.1/4.5	6.4	Malignant/Bx

NHL: Non-Hodgkin Lymphoma; LN: lymph node; FU: follow-up; Bx: biopsy; DLBCL: Diffuse Large B-Cell Lymphoma; HIV: Human Immunodeficiency Virus; HL: Hodgkin Lymphoma; HTLV-1: Human T-Cell Lymphotropic Virus Type 1